Tribology International 177 (2023) 107980

Contents lists available at ScienceDirect

Tribology International

journal homepage: www.elsevier.com/locate/triboint

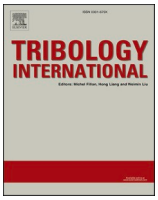

Post-field grinding evaluation of different rail grades in full-scale wheel/rail laboratory tests

M. Mesaritis [a,*], J.F. Santa [b,c], L.F. Molina [d], M. Palacio [d], A. Toro [b], R. Lewis [a]

[a] Leonardo Centre for Tribology, Department of Mechanical Engineering, University of Sheffield, Sheffield, UK
[b] Tribology and Surfaces Group, Universidad Nacional de Colombia, Medellín, Colombia
[c] Grupo de Investigación Materiales Avanzados y Energía – MATyER. Instituto Tecnológico Metropolitano, Medellín, Colombia
[d] Metro de, Medellín, Colombia

ARTICLE INFO

Keywords:
Rail grinding
WEL
Post-grinding performance
Full-scale testing

ABSTRACT

Rail grinding is a maintenance task performed in the field to return it to profile and/or remove damage, however, it can affect the surface integrity of the rail. In this paper, the damage resistance of three different ground rails (R260, R350HT and R400HT) was evaluated. Rail samples were ground using the same parameters in a low-traffic line in the field. The rail metallurgy was then examined, and white etching layer (WEL) formation was evaluated. The resistance to wear and rolling contact fatigue (RCF) was studied in a Full-Scale Rig (FSR). Cracking was detected and, in some cases, WEL was found pressed into the pearlitic microstructure whereas in others the bonding between the WEL and the pearlite failed leading to delamination.

1. Introduction

Rail grinding helps to improve rail life and operation safety while maintenance costs are reduced [1]. The grinding process is performed to remove potential defects that appear during rail's life-cycle and to return its profile. This process, however, involves high levels of stress being applied to the rail material which can cause significant microstructural alteration. The transformed regions of material can affect the performance of the rail due to the irregular mechanical properties.

Based on parameters such as resistance to Rolling Contact Fatigue (RCF) crack initiation and wear, companies have developed and used premium rail grades by introducing a hardening process and/or alloying. Some authors have shown that wear resistance and RCF of hardened rails is improved [2]. Heat-treated rail grades (R350HT and R400HT), for example, have shown to be beneficial for curves with radii up to 3000 m to improve the resistance to wear and RCF [3]. However, given their differences in alloying elements and hardenability it is expected that different grades react differently to the grinding process and the post-grinding run-in.

White Etching Layer (WEL) is a microstructural phenomenon associated with surface damage of steels [1]. In railway maintenance, the WEL is induced at the rail's surface because of the high temperature and pressure reached during rail grinding. The WEL has been reported to appear in both standard rail grades (R260) and hardened rails (R350HT) [3,4]. However, there are no studies available to evaluate if the hardened rails are more or less sensitive to WEL. Moreover, only one study by Cuervo et al. [5] offers some information about the wear and RCF behaviour of heat-treated rails with a WEL. In addition, a significant effort has been made to understand the effect of grinding processes on rail metallurgy and damage at a small-scale in the laboratory. Full-scale laboratory test rig aimed to study and test rail specimens acquired directly from the field can help improve understanding of this topic and fill the knowledge gaps around the subject. The results from this study can be correlated with the small-scale laboratory test previously performed and aid in predicting the performance of the rails after the grinding application.

Accordingly, the aim of this work was to evaluate the response to wear and accelerated Rolling Contact Fatigue (RCF) of three different rails (R260, R350HT and R400HT) with White-Etching layer (WEL) using the pressurization mechanism in a Full-Scale Rig. An exploratory experiment was designed to evaluate if the presence of the WEL on the rails can affect their damage behaviour. The pressurization mechanism has been used to evaluate the response to accelerated Rolling Contact Fatigue (RCF) of different rails in twin disk tests [5,6]. However, to the best of the authors knowledge, there are no reports available using the pressurization mechanism in a Full-Scale Rig. This study aimed to

* Corresponding author.
E-mail address: mmesaritis1@sheffield.ac.uk (M. Mesaritis).

https://doi.org/10.1016/j.triboint.2022.107980
Received 7 April 2022; Received in revised form 2 September 2022; Accepted 3 October 2022
Available online 6 October 2022

Table 1
Chemical composition of rail and wheel samples (wt%) [7].

	C	Si	Mn	P	S	Cr	V	Cu	Ti	Ni	Mo	Tensile strength/MPa
R260	0.736	0.270	1.056	0.032	0.023	0.026	0.003	0.002	0.016	0.021	0.006	≥ 880
R350HT	0.739	0.453	1.198	0.016	0.013	0.085	0.001					≥ 1175
R400HT	0.931	0.251	1.269	0.009	0.022	0.275	0.0035	0.017	0.002	0.015	0.0068	≥ 1280
E8	0.542	0.253	0.734	0.011	0.006	0.141	0.006	0.165	0.002	0.120	0.048	860–980

Table 2
Grinding parameters used for the tests.

Parameter	Value	Pattern	Angles and pressure distribution
Travelling speed (km/h)	6 ± 1	23	31°G-(70%), 26°G-(70%), 21°G-(70%), 16°G-(70%),10°G-(70%)
Rotational grinding stone speed (rpm)	6600	24	12°G-(70%),9°G-(70%),6°G-(85%),3°G-(85%),0°-(85%)
Number of stones	5	25	3°G-(85%), 1°G-(85%), 0°-(85%), 1°F-(85%), 3°F-(85%)
Number of passes	32	28	11°G-(70%),8°G-(70%),5°F-(85%),2°F-(85%),1°F-(85)
Maximum depth of removal (mm)	0.5	29	0°-(85%),3°F-(85%),6°F-(85%), 9°F-(85%),12°F-85%)
Profile type	CPF: contact profile field [9]		

simulate the post-grinding conditions that exist in the field and study the performance of the ground specimens. The analysis included the determination of the differences in the coefficient of friction as well as the roughness development throughout the duration of the experiments. Moreover, these experiments aimed to explore the material transformation effect that occurs on the top layer of the rail and identify how this affects the performance of the rail. An assessment of the microstructure at the areas of WEL before and after the experiments took place to study the phenomenon. Summarizing, the effect on various rail grades and the post-grinding evolution of roughness and wear in a full-scale laboratory environment was studied.

2. Methodology

In this section the specimens used for the testing are presented along with the testing methodology followed.

2.1. Materials

Specimens acquired from the field were from grade R260, R350HT, R400HT rails. The chemical composition of the rails measured by Optical Emission Spectrometry (OES) and the tensile strength of the rail specimens are presented in Table 1.

2.2. Grinding tests

The grinding of the rails was conducted using a Harsco RGH10C rail grinding train. The rail grinding machine has 5 resin bonded 6-inch aluminium oxide (Al_2O_3) stones on each side with grain size of 16 abrasive particles/cm^2. A peripheral face grinding process is performed using the machine with an attack angle between + 45° and − 40°. This angle is defined as that of the cutting face relative to the work.

Grinding parameters used for the experiments are presented in Table 2. These parameters follow a regular pattern used for treating the rails in a preventive maintenance approach. This grinding process involved the removal of a predetermined amount of material over a number of grinding passes. This approach is used to remove the normal wear and lessen the likehood of rail failure. The grinding patterns described are measured along the rail head's perimeter from the rail axis toward the gauge (G) or the field (F) zone [8]. The percentage of power (% Power) used during the grinding operation is an indirect measurement of the pressure and it represents the available power in the motors. More details about the grinding patterns can be found elsewhere [8]. The grinding experiments occurred on the CPF (contact profile field) rail section as indicated in Fig. 1. This was done to ensure geometry compatibility of the field samples with the Full-Scale Rig for the post-grinding rolling/sliding testing.

Brand new 6-metre rail sections of R260, R350HT and R400HT grades were installed in a low-traffic line of Metro de Medellin as shown by the scheme in Fig. 1. After the completion of the grinding process, samples were extracted from each rail grade using a lubricated band saw.

The specimens were then machined down to pocket size specimens to fit in a pre-configured rail in the Full-Scale Rig used for post grinding damage tests. Dimensions of the specimen are presented in Fig. 2.

2.3. Full-scale rig

Similar to real-life conditions, where ground rails are used for a prolonged time until the subsequent maintenance, the ground specimens

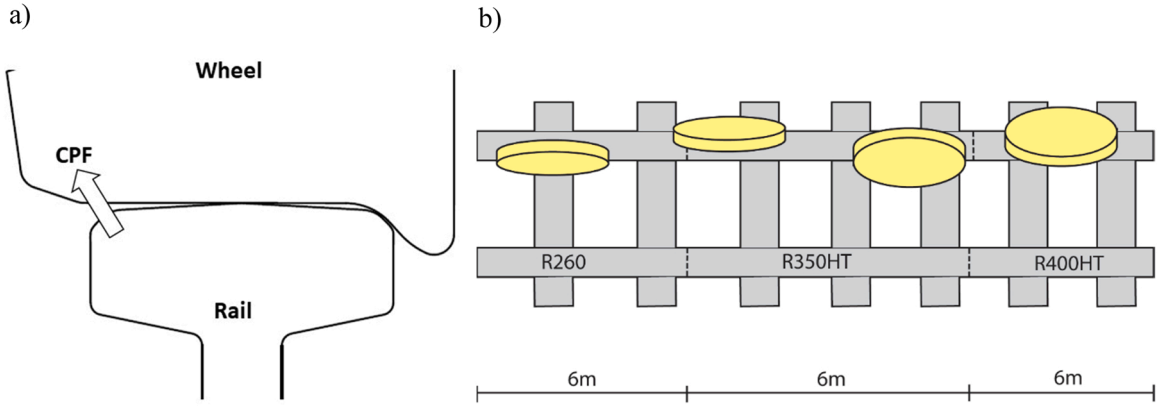

Fig. 1. a) Representation of the wheel/rail CPF (contact profile field) contact mode where grinding was executed; b) Scheme of the configuration of the grinding process [9].

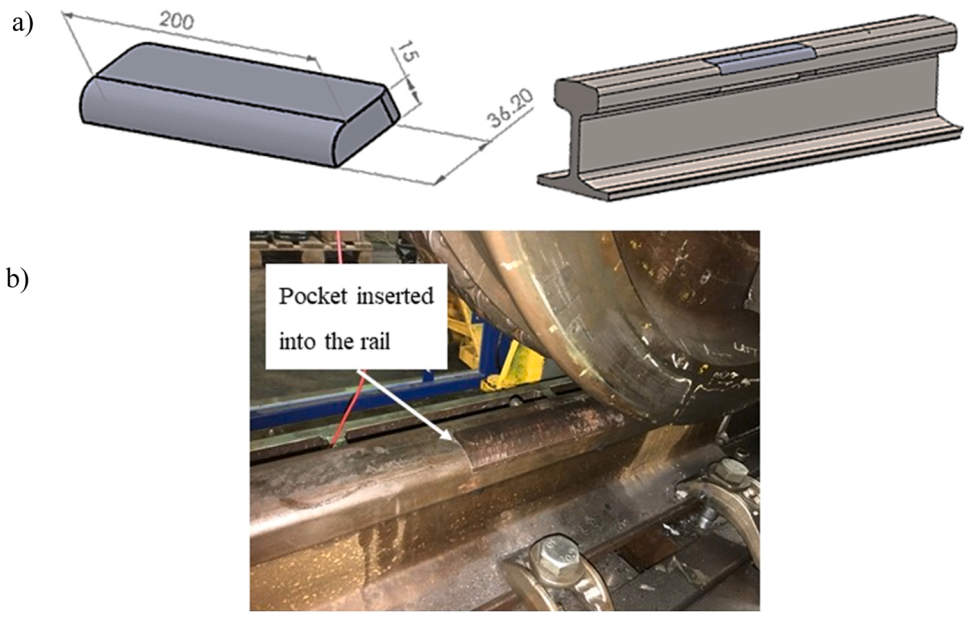

Fig. 2. a) Dimensions of the specimens and samples (in mm); b) Representation of the specimen inserted into the pocket.

needed to be tested in a wear/rolling contact fatigue test to determine the post-grinding performance. The testing facility used for this study can simulate real-life conditions that exist in the field. The rolling contact experiment was carried out to generate wear and cracks on the specimens simulating similar damage of rails in the field. The test rig utilises an actual rail, identical to the ones used in the field with a pocket to accommodate the ground specimens. A wheel acquired from the field can roll over the rail applying the required load and the pre-determined slip. The results shown in this work describe the average behaviour recorded. During the testing the shear force was captured between the rail and wheel and used to calculate the coefficient of friction on the contact area. The load was applied on the wheel at the beginning of a cycle. The load applied to the wheel was 110 kN through a load cell implemented on the vertical actuator to obtain a contact pressure of 1300 MPa. The contact pressure was determined using an ultrasonic contact pressure map for the FSR from a previous study [10]. The total moving distance used in this study was 400 mm. Throughout the test, the laboratory temperature was between 24.1 °C and 26.1 °C, and humidity varied between 24% and 36%. More information about the FSR can be found elsewhere [11,12].

The dry testing was run for up to 12,000 cycles. Following this, a lubrication system was used to introduce water into the contact area for another 8000 cycles to pressurize the cracks. The contact pressure was 1300 MPa, rail velocity 100 mm/s and slip 2%. To introduce lubricant into the contact area a drip feed system was added to the test rig that provides 1 drip every 7 s. The droplets were applied on the top of the wheel and, through gravity, ran towards the contact area.

Another aim of this study was to monitor how roughness develops throughout the test and what impact this might have on the coefficient of friction between the wheel and rail. The rail specimen used was previously ground whereas the wheel disc had a fresh surface. The coefficients of friction were monitored in the test, and the surface roughness Ra parameter was determined at intervals during the test by using the replica acquisition procedure described in [13] (and below). The Ra parameter was used to describe the roughness development as it is the most commonly used parameter to determine compliance of the rail roughness with the standards. The roughness Ra parameter was measured at 50 and 100 cycles and then 100 cycles up to 600 cycles.

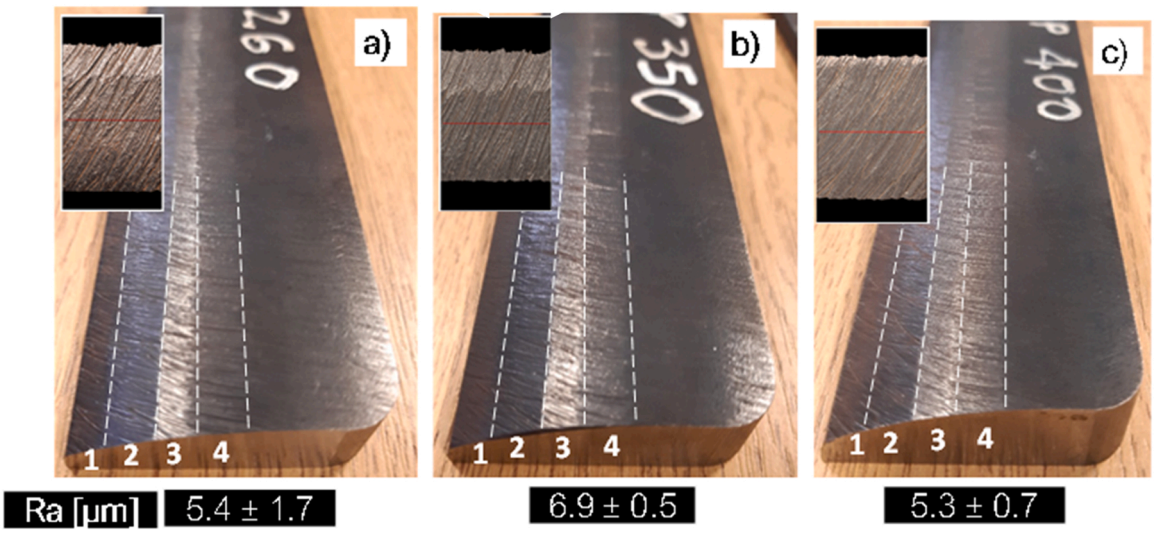

Fig. 3. Ground specimens before full-scale testing.

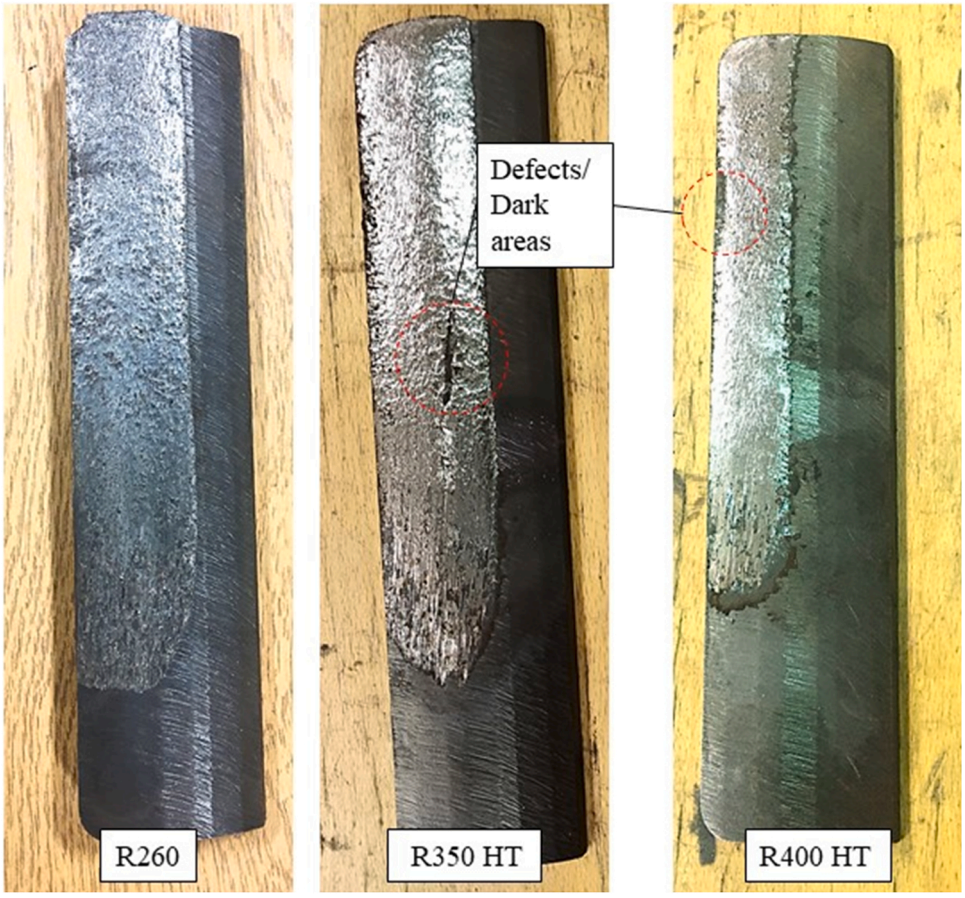

Fig. 4. Ground specimens after testing.

After that data were taken every 200 cycles up to 1000 cycles. Little change was observed between the roughness measurements so then data was taken at 5000, 12,000, 17,000 and at the end of the 20,000 cycles. The procedure followed for the surface roughness measurements is described below:

- Stop the test.
- Clean the specimen with an acetone spray.
- Apply a layer of Microset 101 Thixotropic replicating compound to the disc's surfaces, before adding a piece of backing paper, and waiting six minutes for the replica to set.
- Use an Alicona InfiniteFocusSL 3D measurement system with a 5X magnification lens and a cut-off wavelength of 800 μm to create a digital representation of the surface of the replica.
- Choose lines with a minimum length of 4 mm on the digital image along which the Alicona software calculated roughness measurements.
- Clean the specimen with acetone spray.
- Continue the experiment.

2.4. Analysis of ground rail specimen's metallography

Specimens were sectioned before and after the tests, polished and etched in 2% Nital to allow examination of the microstructure using both optical and scanning electron microscopy.

A Bruker Hysitron TS 77 with a Berkovich intender along with a 2500 μN force was employed for this experiment. An indentation method was used with 2 μm distance between points to create a dense cluster of indentations that would verify the existence of WEL. The area tested is presented in Fig. 12 a). The testing allowed the acquisition of nano-hardness of the area. The raw data initially obtained are the load-displacement of the indentations which were further used to calculate the mechanical properties. Individual points were then utilised to create a heat map.

3. Results

3.1. Surface analysis

Observing the rail specimens prior to the testing, four distinguishable facets were identified, as shown in Fig. 3. These were created from the grinding pattern utilised. After the testing a worn area appears on top of the specimen as it can be observed in Fig. 4 indicating the zone slip was applied during the testing. By identifying these facets, a more specific analysis can be done for the microstructure and roughness data along the affected facets before and after the testing. Comparing the surface with Fig. 3 it can be clearly seen that the specimens have experienced significant wear during the testing. The increased amount of wear is partly due to the lubricated cycles introduced during the final 8000 cycles of the experiments. The low viscosity of the water penetrated the cracks that were formed in the initial 12,000 dry cycles. This accelerated the fatigue crack growth by the action of hydraulic pressure [14].

Another fact that can be identified by the observing Fig. 4 is the difference in the surface topography among the rail grades. There is a distinguishably rougher surface on the R260 compared to the R350 HT and R400HT grades. This was expected as the latter two rail grades exhibit higher hardness levels that translate into higher resistance to plastic deformation. Further comparison of the roughness and the surface profiles will aid in the validation of this argument.

Some external defects were identified after the completion of the experiments (highlighted in Fig. 4) in the R350HT and R400HT grades. Since the grinding process could have been a contributing factor to the

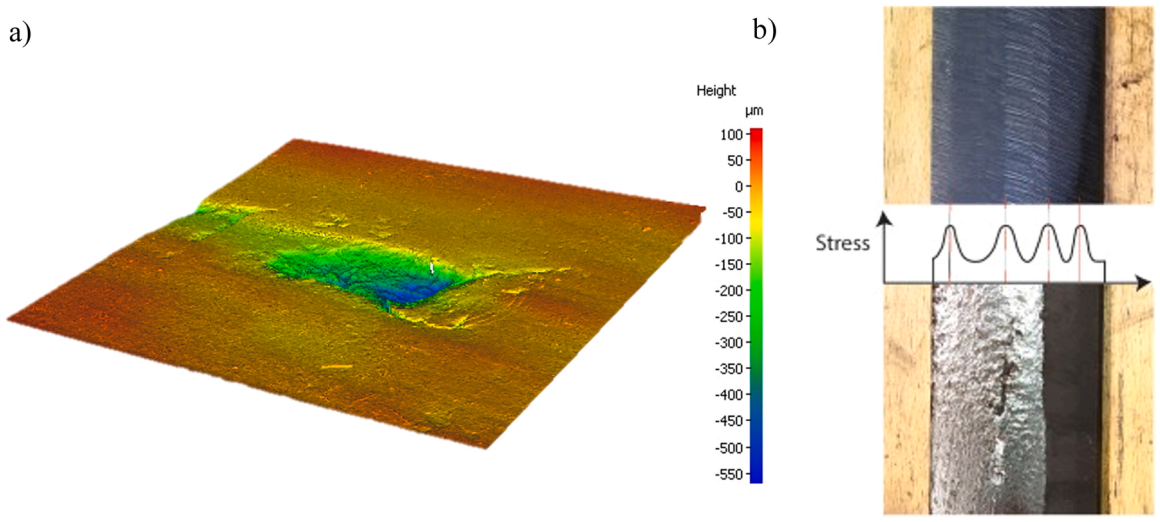

Fig. 5. a) Representation of the topographical profile of R350 HT defect, b) Illustration of the stresses distribution on the facets of R350 HT.

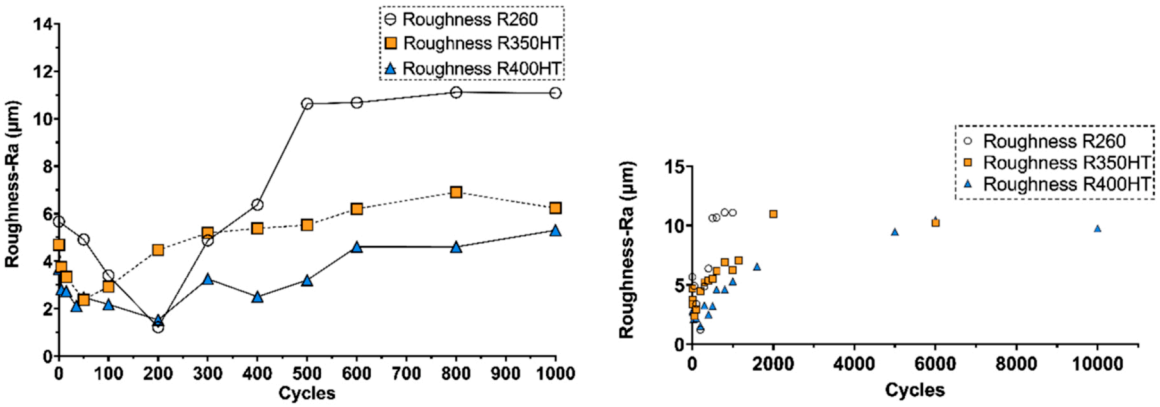

Fig. 6. Ra roughness parameter development during the test.

formation of these defects, further analysis was carried out.

Further analysis was done only on the R350HT profile as the defect on the R400HT was on the edge of the specimen indicating that the material loss might not resulted by the rolling/sliding experiments but due to the interaction between the pocket and the rail. The 3D profile of the defect found in the R350HT rail was acquired to determine its morphology. This allowed identification of any correlation with other similar defects found in the field and the determination of possible causes. Fig. 5a) shows the 3D surface topography representation of the area around the defect acquired using an Alicona Infinite Focus SL 3D microscope. Visually the surface image displays dark areas at the location of the defects. The distinguishing factor between the defect and the rest of the worn surface is the morphology of the surface on the dark areas. A cross section of the defect would reveal any signs of plastic deformation below the black spot area and other features such as crack paths. The variance of the shape and size of the defect compared to defects detected in other studies [15] could be the result of the slightly different mechanics within the full-scale test rig compared to the field. Another consideration is the topography of the specimen and the smoothing-out process of the asperities. Fig. 5b) superimposes the initial ground surface of the R350HT specimen against the worn surface upon completion of the testing. Observing the images, a correlation between the grinding facets and the location of the surface defect can be detected. As the grinding occurs, a number of grinding stones are utilised to accomplish reprofiling of the required shape resulting in a surface with facets as shown in Fig. 3. An edge is formed at the area where two facets meet creating a point of stress concentration during the consecutive wheel passes as shown in Fig. 5b).

As previously mentioned, replicas were acquired throughout the experiments to monitor the development of surface roughness and identify any potential correlation with the CoF. Small cycle intervals were performed up to 1000 cycles where most of the fluctuations occurred. The initial roughness of the specimens differs, with the R260 specimen exhibiting the highest roughness and the R400HT the lowest. Again, this was expected as the harder materials will exhibit the least abrasion/deformation during the grinding process, hence the least surface disruption. This was then followed by the smoothing of the asperities and surfaces reaching the lowest roughness, that was then succeeded by the initial stages of wear and potentially WEL removal leading again to an increase in roughness. For the R260 and R400HT specimens the lowest roughness was detected at 200 cycles and for the R350HT at 50 cycles.

The roughness of all specimens then increased gradually until it stabilised. As presented in Fig. 6, measurements up to 10,000 cycles were taken at larger intervals to identify the maximum roughness reached in each case. Although all the specimens in terms of roughness converged around 10 µm, small differences were perceived regarding the highest actual roughness value and the time required for the roughness to converge. In terms of the time required for the roughness to converge the R260 specimen reached its highest value significantly earlier than the other samples, at 800 cycles and remained stable. The R350HT converged after 2000 cycles with the R400HT specimen

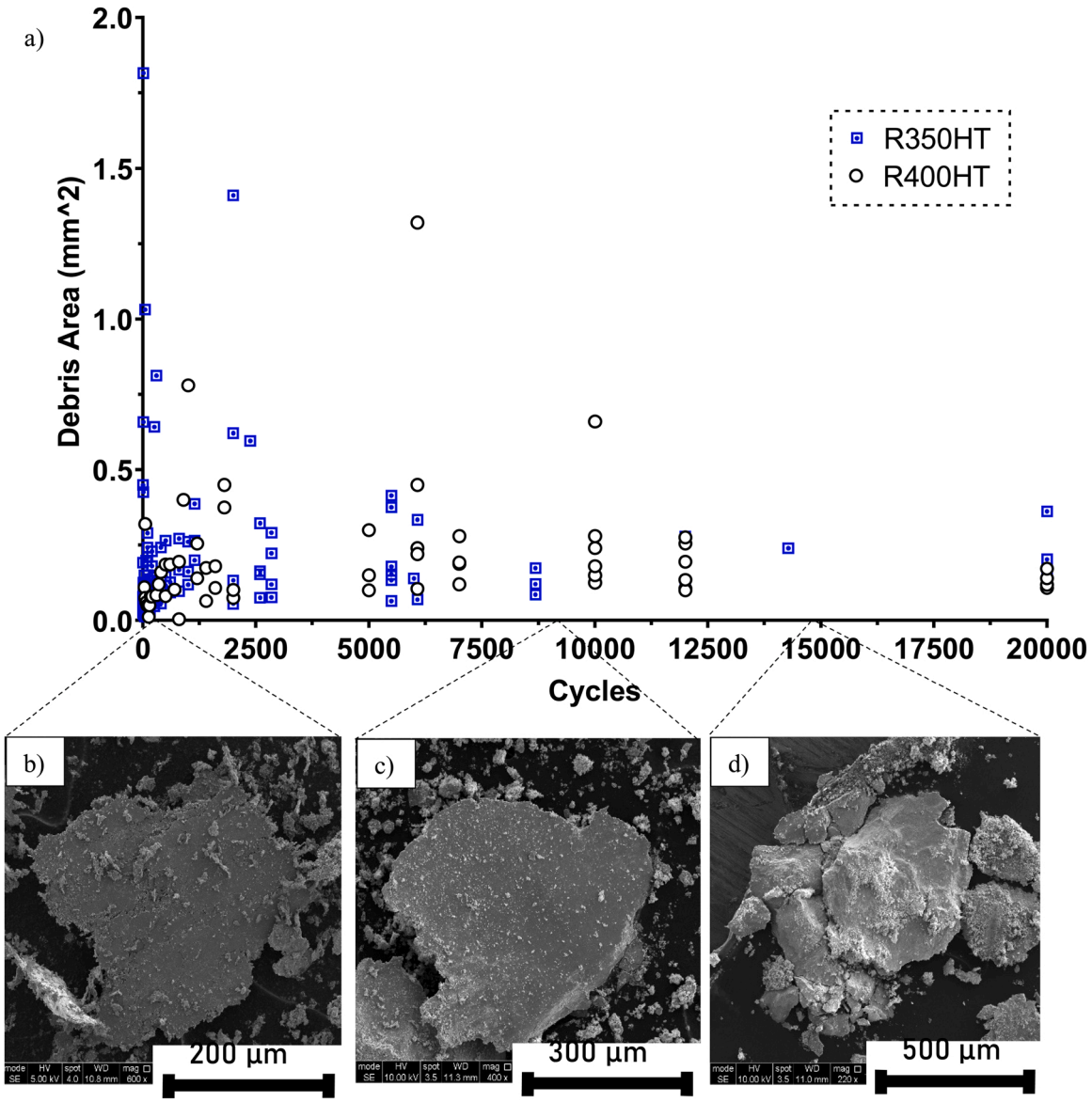

Fig. 7. a) Illustration of the size development for the R350HT and R400HT debris. SEM images of debris: b) 200 cycles from R400HT sample; c) 8685 cycles from R350HT sample; d) 14280 cycles from R350HT sample.

requiring the longest time to converge at 5000 cycles. As mentioned previously it is presumed that the roughness development and converging time is dictated by the hardness of the material. Furthermore, the behaviour observed in all three grades, reminiscences the typical roughness-development-over-time curve of machined surfaces produced by Blau et al. [16] which have three distinct regions, the run-in, the mild wear/steady-state and the transition to more severe wear.

Debris was collected throughout the experiments at specific intervals. Due to the equipment limitations, the current analysis was performed on the R350HT and R400HT specimens only. Nevertheless, the results presented would allow a potential correlation between the debris area and the roughness values. As various debris samples were collected at each interval, Fig. 7 presents the entire data acquired and analysed. During the first 150 cycles of the experiments the debris' calculated areas were concentrated between 0.03 and 0.11 mm^2. There were some isolated measurements with significantly higher calculated areas compared to the rest. This could be due to the asperities smoothing and occasional fracture of some. Following the initial run-in, the debris ranged between 0.08 and 0.2 mm^2 indicating an increase in the size of debris. These measurements are in agreement with the rise in roughness values after the first 200 cycles indicating that the specimens transitioned into a wear region. As the cycles progressed the average debris size fluctuated between 0.13 and 0.3 mm^2 with sudden spikes occurring occasionally.

Regarding the morphology of the debris, distinct differences were observed between the debris during the initial cycles and the final cycles. As it can be seen in Fig. 7, up to 6000 cycles the debris is reminiscent of flakes released from the ground surface. This indicated that the tribo-system was still attempting to reach a steady-state condition by smoothing and removing the asperities created during the grinding process in a ratchetting type process. During this stage the system was within the run-in/mild wear region based on the Blau et al. [16]. After 6000 cycles the morphology of the debris changed indicating that the specimen had entered a more severe wear region as fracture is presented in the debris as displayed in Fig. 7d). This comes in agreement with the data observed in Fig. 6 where theR400HT roughness reaches a peak at 6000 cycles. Another observation in Fig. 7b) and c) was the sub-micron particles bonded on the surface of the debris. This is another indication that the debris were most probably detached from the ground surface,

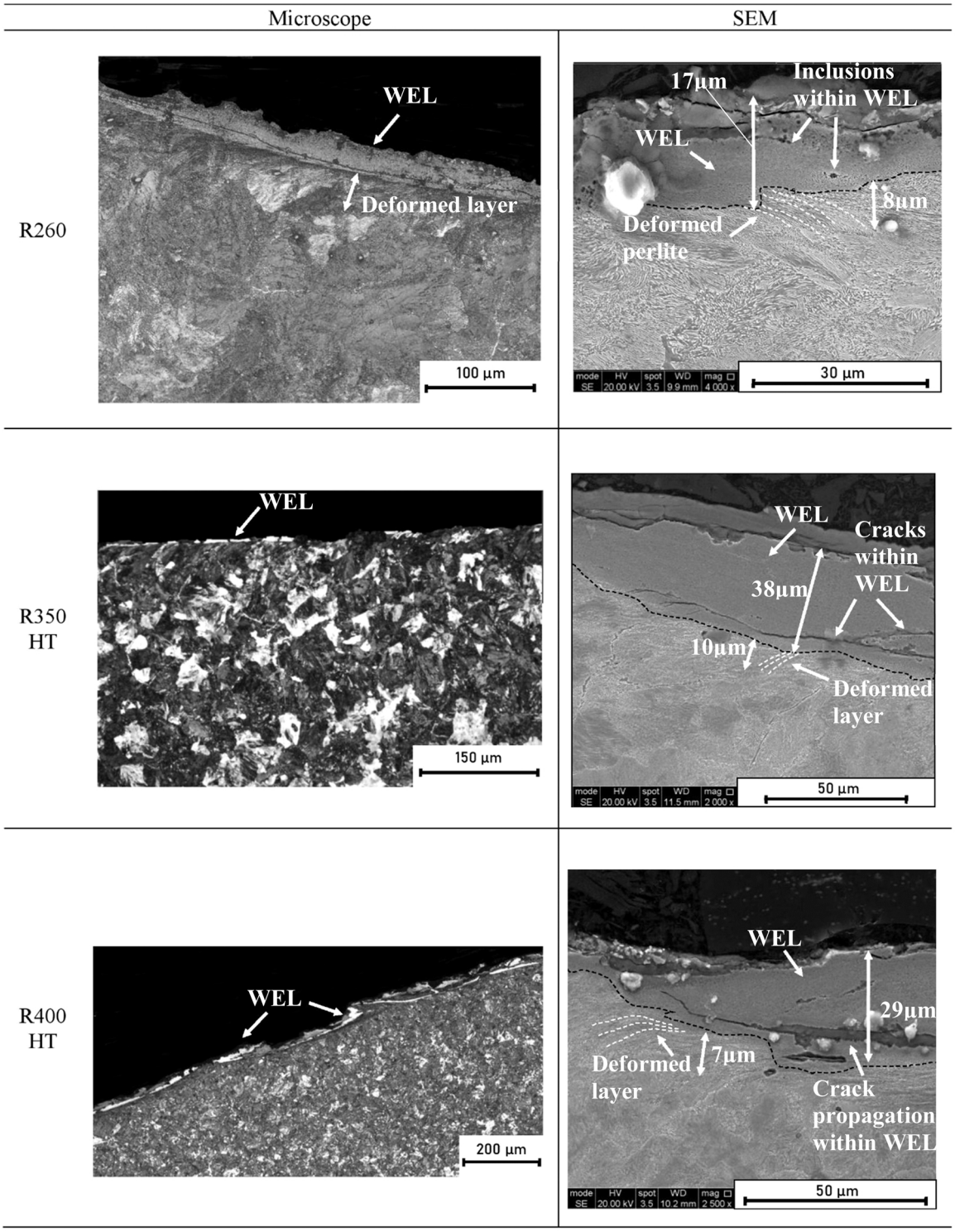

Fig. 8. Optical and SEM images of rail specimen microstructure after grinding and before full-scale tests.

which was interacting with the environment, hence the presence of oxide particles.

3.2. Microstructure analysis

3.2.1. Microstructure after grinding tests

The microstructure of R260 rail after the grinding process and before the full-scale tests is presented in Fig. 8. A WEL was developed due to the grinding process. The maximum thickness of WEL that was found in the samples was 45 µm. Below the WEL a significantly deformed pearlite layer was detected indicating the substantial amount of energy that was input during the process. The thickness of this transition layer fluctuated between 2 and 11 µm.

The same analysis was performed on the R350HT sample before it was tested to assess its microstructure. Similar features were detected in this case, such as the presence of WEL and a transition zone right below followed by deformed pearlite. In this case the maximum thickness of WEL detected was 40 µm and only on very short lengths. The most

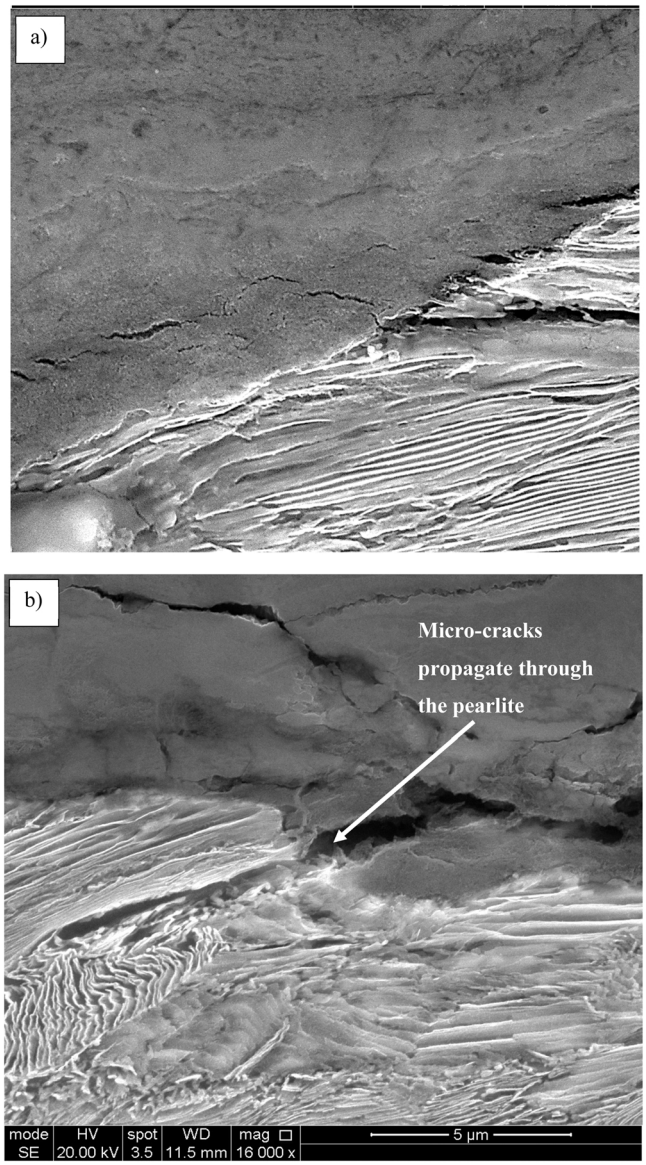

Fig. 9. SEM images of: a) R260 field rail samples after grinding representing areas where microcracks went through pearlite; b) Cracks initiated withing the WEL and progressing to pearlite.

consistent thickness observed was 13 μm for the WEL and a range between 8 and 11 μm of deformed layer. Severely deformed pearlite layers were found in some areas that were broken down to smaller pieces within the WEL. This resulted in a severely deformed pearlite microstructure that exhibits numerous cracks with scattered pieces. Compared to the R260 sample this specimen shows slightly higher resistance to WEL formation with larger areas being plastically deformed.

The final specimen that was analysed in terms of its microstructure was the R400. The specimen was extracted after it was ground under the same parameters as other specimens. As expected, this sample showed the existence of WEL as well as indicating that the effect of grinding is applicable to all rail grades regardless of whether being heat treated or not. Nevertheless, distinguishable differences were found in these samples such as smaller transition layer that appears in-between the WEL and bulk material. Attributable to the higher hardness of the current specimen, hence higher resistance to plastic deformation, only a small part of the shear forces could be absorbed by the bulk material. The average value for the transition zone thickness is around 7 μm, with the average thickness of the WEL ranging from 15 to 20 μm. A maximum

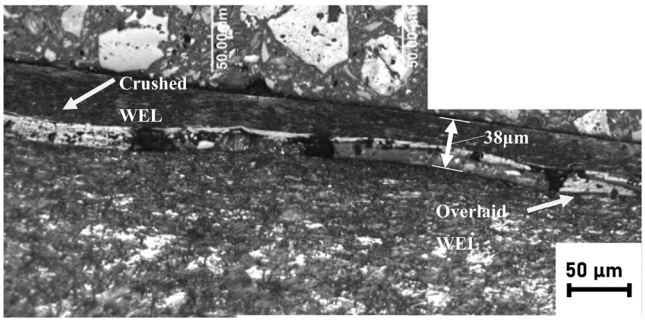

Fig. 10. WEL overlaid by the deformed pearlite upon completion of the FSR experiments.

thickness of WEL was identified at 34 μm, however its existence was limited to a very short distance of around 38 μm. Additional details related to the angular distribution and the statistical analysis of the WEL of the three rail grades can be found elsewhere. All the measurements for the WEL thickness and the deformed layer were taken from the SEM images as they offered more precise resolutions.

Due to the various defects spotted in the initial WEL images some further analysis was required to acquire more information. Therefore, images were taken of specific areas of WEL to study the defects and their effect on crack propagation. Numerous cracks presented in and around the WEL of the R260 sample are shown in Fig. 9a). In most cases, the cracks started from the top-running surface and moved towards the bulk material with no clear indication of their initiation point. Fig. 9a) exhibits cracks that managed to propagate towards the pearlite matrix initiating cracks into the bulk material. Although it is not clear what caused these cracks, other studies [6,13] stated that this transformed layer exhibits significantly higher hardness levels that can lead to a brittle layer which is more susceptible to crack initiation. Cracks could be initiated at any depth in the WEL and propagate down into the rail following the direction of the deformed sheared grains. Fig. 9b) presents SEM images of the R350HT at higher magnification, showing a crack initiated from the WEL area and propagated down to the pearlite matrix. Similar to Fig. 9a), the crack follows the direction of the deformed grains as the easiest possible crack propagation route into the pearlite structure.

3.2.2. *Microstructure after full-scale testing*

Upon the completion of the full-scale rolling/sliding experiments the specimens were sectioned and polished to be prepared for metallurgical analysis. Images of the sectioned specimens are presented in this section. In Fig. 10 the image of R400HT shows that the WEL has been overlaid by deformed pearlite. The formation of this figure was done by combining together a number of microscopic images in an effort to showcase these microstructural features and identify its root cause. Results from another study [17], exhibited similar results by displaying WEL overlaid by deformed pearlite after rolling/sliding testing. However, the existence of WEL below the deformed material was not distinguishable on a microscopic level. In this case, the amount of the remaining WEL is significantly larger and visually distinguishable on a larger scale. As the parameters used in the grinding process, the full-scale rolling/sliding experiments and during the preparation of the samples were identical it can be said that the variation in the mechanical properties of the R400HT could be the deciding factor for the increased amount of WEL observed. Other factors that could result in the larger amounts of WEL presented are the bonding mechanism between WEL and the various rail grades as well as variations of WEL between the rail grades. Further analysis needs to occur to clearly define the key factors resulting in this phenomenon.

As a ground rail with a phase transformed layer progresses throughout the running cycles two possible scenarios might occur: 1) the

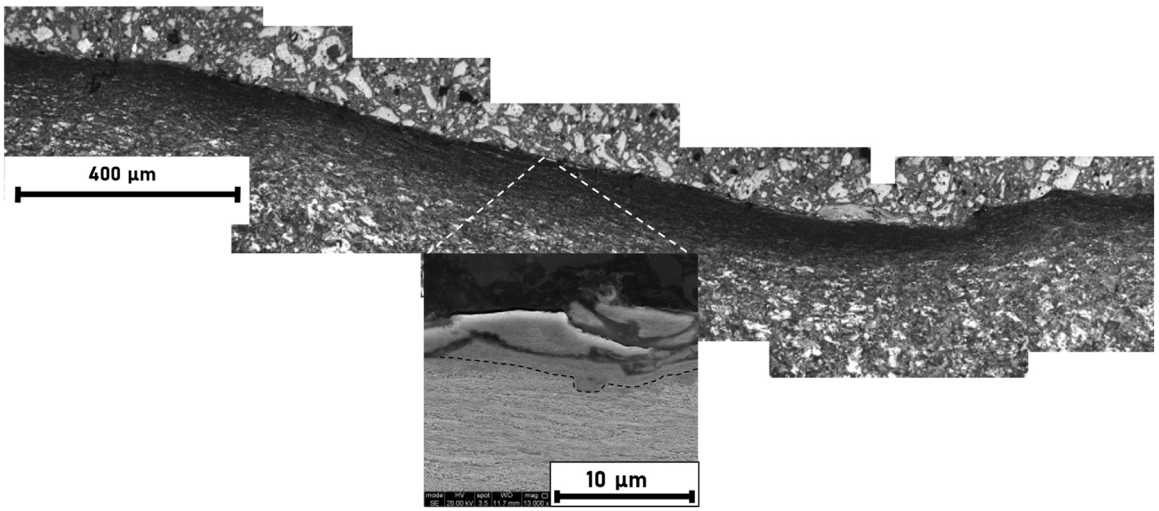

Fig. 11. Cross-section of the defect detected on the R350HT specimen.

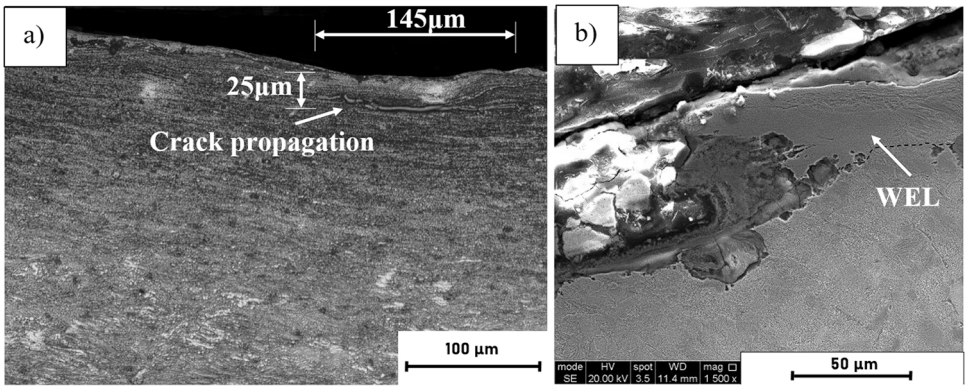

Fig. 12. Images after the testing on the R260 sample showing extensive deformation.

WEL could be pressed into the pearlitic microstructure applying significant pressure to the bulk material to accommodate the martensite layer; 2) destruction of the bonding between the WEL and the pearlite leading to the delamination of the martensite layer. The image of R400HT in Fig. 10 falls within the first scenario. Since the martensite exhibits much higher hardness levels than pearlite, the later succumbs to the pressure from the WEL layer and deforms to accommodate the WEL remaining. Moreover, the figure shows in some areas the propagation of cracks along the rolling direction which could result in the formation of the defects. This implies that the encapsulated WEL could have a negative impact on the crack formation and the general formation of defects on a post-ground rail. Furthermore, in some other areas the remaining WEL was crushed by the top pearlite layer and the load applied from the rolling wheel creating many small martensite fragments.

A cross section of the defect detected on the surface of R350HT sample and displayed in Fig. 4 is presented in Fig. 11. Images obtained aimed to provide further information and allow the identification of the root cause. The main information obtained from the microstructural analysis was the deformed pearlite layer which continued from the running surface to the defect area. This implies that the plastic deformation existing might have occurred due to the friction between the crack faces prior to detachment of the top piece or due to direct contact between the rail and wheel upon detachment. Considering the information obtained, the defect could be associated with the spalling defects. As spalling is a material loss defect similar to flaking and shelling, but it is more localised and it tends to produce much shallower defects in comparison with the others [18]. Flaking was not considered as it occurs

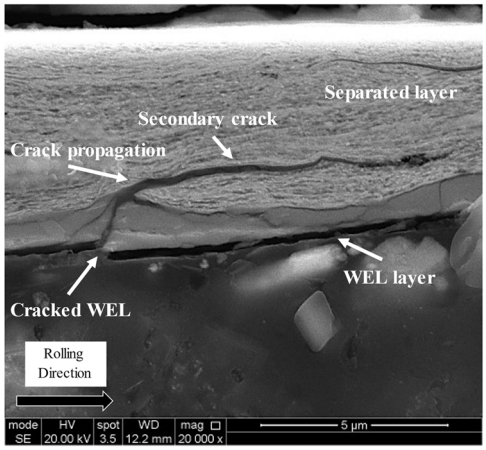

Fig. 13. SEM images of R400HT sample after the experiments displaying the effect of WEL on crack propagation.

in the gauge corner of the rail and this defect was detected in the running band of the rail [19]. It can be also seen that the R350HT sample contains WEL on the top running surface. The high contact stress from the grinding roughness and the brittle nature of martensite layer could aid in the breaking and spalling effect of fragments from the bulk material.

The results from the R260 specimen are presented in Fig. 12. Optical microscope and SEM images were taken at higher magnification in

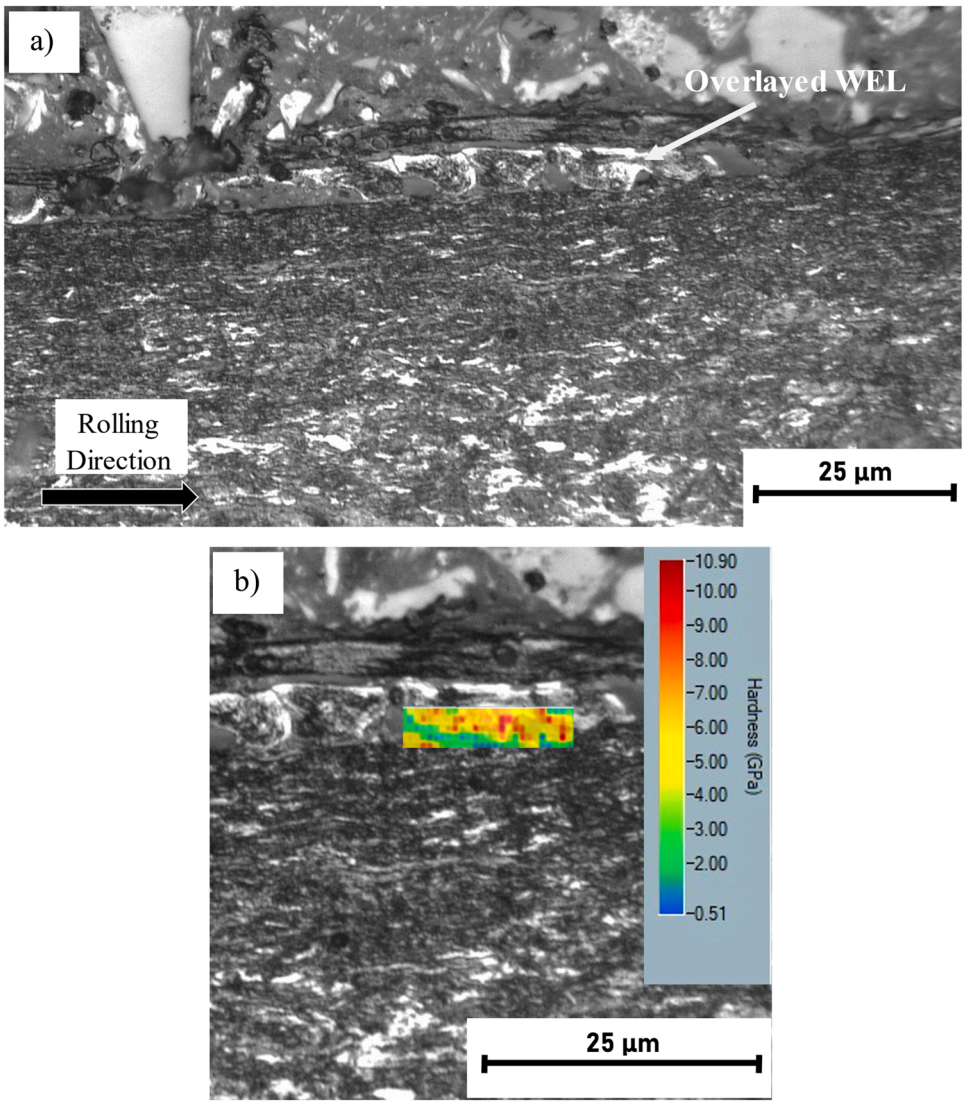

Fig. 14. a) R400HT microstructure from an optical microscope exhibiting overlaid WEL; b) Nanoindentation mapping performed on the embedded WEL in the R400 HT.

specific areas of interest. The optical microscope images display clearly the plastic deformation due to the rolling/sliding. Fig. 12 a) exhibits crack propagation as a result of the shear stresses the material endured. Fig. 12b) demonstrates the delamination of WEL with minimal impact on the pearlitic structure compared to the other case.

Fig. 13 demonstrates the effect of WEL on crack propagation in post-grinding rolling/sliding experiments. The brittle nature of WEL initiates cracks within the layer that propagate towards the bulk material. Additionally, in both instances the cracks are initiated from the WEL that was initially overlaid by the deforming pearlite and eventually detached due to the rolling/sliding mechanism. The separation of the upper pearlite layer could result in the weakening of the upper layer structure and in combination with the brittle nature of WEL, the layer can be more prone to crack generation. Thus, this suggests that the overlaid/encapsulated WEL and consequently the presence of WEL in general can impact negatively on the life-cycle of a rail by encouraging the formation of cracks.

To verify the existence of WEL a nano-hardness test was performed on an area of the R400HT specimen where overlaid WEL was detected. The hardness map presented in Fig. 14 b) clarifies the existence of harder material as it demonstrates significantly higher hardness values within the area WEL as was initially speculated to exist. The WEL values varied between 7.5 and 10.9 GPa (765–1111HV).

3.3. Wear and friction data

Fig. 15 represents the wear rate against Tγ/A index obtained from the current experiments. Using the Tγ approach allows consideration of wear and fatigue in a single parameter. The wear number (Tγ) represents the energy consumed in the wheel/rail contact area and does not differentiate between various forms of energy (heat, noise, wear etc.). Hence wear maps can be created by analysing wear data and help draw to conclusions on the performance of the rail samples. Additional data attained from a study by Eadie et al. [20] point where an experiment was done with a full-scale fresh sample made of R260 rail grade and tested on a similar kind of full-scale test rig were used as a reference. It should be noted that the parameters of the experiment were different with a slip of 0.5% and 1 GPa pressure was applied for 100,000 cycles. As expected, the results presented followed the pattern where the lower hardness materials exhibit higher wear rates and vice-versa. However, what needs to be noted is the higher wear rate demonstrated on the experiments with the ground R260 full-scale sample compared to the freshly manufactured one. Although parameters are different, thus the shear forces applied to each specimen varied, it can be said that the topographical

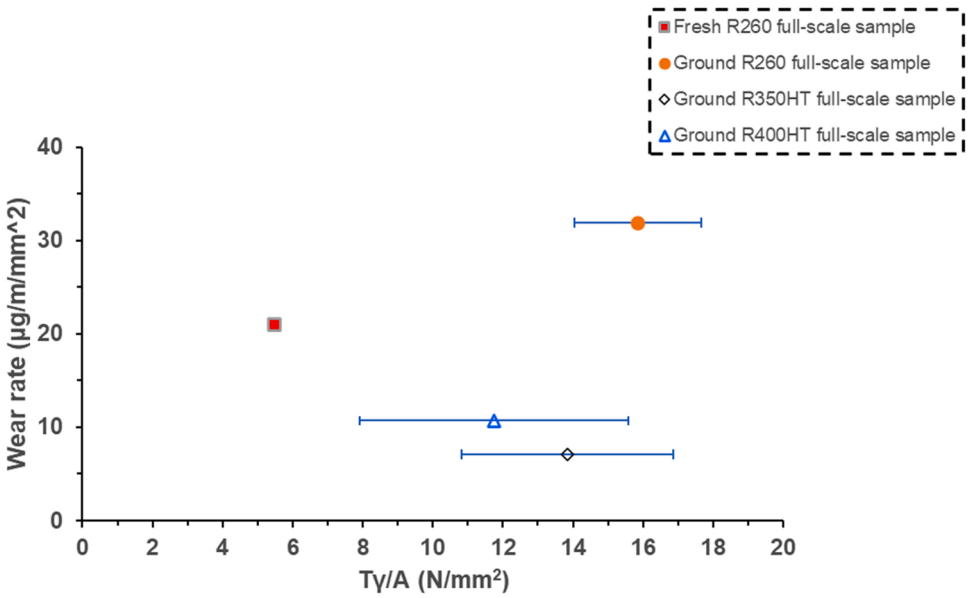

Fig. 15. Wear rates from the testing of ground surfaces compared with a full-scale test performed with fresh surface specimen for 260 grade rail.

distortion combined with the subsurface microstructural features left by the grinding process could affect the life-cycle of the rail. Nevertheless, further tests need to be done under identical parameters to examine the effect of grinding on the specimens post-grinding wear rate.

The coefficient of friction (CoF) registered during the tests for the different rails is very similar. The running-in for the three different rails grade was around 3000 cycles. In this case, the running-in is analysed as the period with time-dependent variations in friction force [21]. After 3000 dry cycles, the CoF was stable and varied in the range between 0.30 and 0.35. When water was applied to the contact the CoF was reduced, and the value varied from 0.17 to 0.30.

Generally speaking, in wet tests the R260 demonstrated the highest CoF (0.25–0.30) while the lowest CoF (0.17–0.25) was observed for the R400HT with the R350HT lying in the middle (0.23–0.27). It can be said that the initial rougher surface resulted in an increased CoF between the wheel/rail interface for the R260 and R350HT specimens. Furthermore, the hardness levels of each material might affect the CoF levels since a harder material would resist more to plastic deformation affecting the profile and the entire contact area between the two bodies [22].

4. Discussion

Data acquired as part of this study displayed interesting information with regards to the post-grinding performance of rails. Prior to the experiments the specimens were extracted directly from the field after the occurrence of a grinding process. As mentioned previously, these results will aid in the improvement of the rail grinding efficiency and in the alternation of the grinding parameters to improve surface quality.

The initial images presented in Fig. 4 showed a more worn surface on the R260 specimen, but a flaking effect occurring on the harder materials. Smaller interlamellar distance occurs can result in rails being more susceptible to cementite dissolution hence crack propagation [23]. Considering this in combination to the presence of a brittle martensite layer leads to the conclusion that harder rails could suffer more from squats compared to standard rails due to the easier crack propagation through brittle structures [24]. Moreover, the surface finish on harder steel materials does not smooth out as easily as in the softer R260 specimen resulting in stresses being applied over the facet edges for extensive time periods compared to the areas in-between as shown in Fig. 5b). Combining this information with the possible existence of martensite around the facet edges increases the chances of crack formation during the run-in due to the brittle nature of WEL and the increased stresses applied to it. Similar findings were reported by Rasmussen et al. [25] in a field study aiming to explain the periodic cracks detected in an R350 HT rail. The explanation given included the induced hard and embrittled martensite that can initiate cracks easier and the concentrated stresses along the facet edges which are applied for longer time on harder rails.

The metallurgical analysis that was done on all specimens verified the existence of WEL. It was clearly shown that the transformation of the pearlitic microstructure to a martensitic layer occurred due to excessive plastic deformation and heat energy dissipated by the grinding process [26]. Furthermore, a variance was observed between the thickness of WEL on the different rail grades with the R260 exhibiting the thickest layer at 45 µm in short specific patches and the R400 HT the least. As the grinding process is a dynamic procedure where the environment is constantly changing, the wheel breaks down from use and rail profile continuously fluctuates; hence the control of the pressure applied through the grinding wheel and the depth of cut could be compromised leading to larger amounts of transformed WEL. Therefore, although the results show larger quantities of WEL on the R260 further testing should be done to verify the results.

The amount of transformed martensite is partly governed by the amount of heat dissipated to the pearlitic microstructure. Moreover, it has been proved that the dissipation rate can be dictated by the interlamellar spacing of the pearlitic microstructure [20,21]. As the R400 HT is a heat-treated pearlitic structure with refined grains to make the structure harder and more resistive to wear as a consequence it has a smaller interlamellar distance, resulting in higher heat dissipation rates. In a grinding process this translates to heat dissipated through the contact area that would reach deeper levels towards the bulk material. Subsequently the amount of material that would go through the austenitisation and recrystallisation process is greater, leading to the larger amounts of WEL. Nonetheless, other factors such as the external environment and the amount of heat in the contact area can affect the depth of austenisation, hence further experiments need to be conducted to examine the effect of the interlamellar spacing. Additionally, it has to be noted that the austenitisation temperature varies depending on carbon content of the rail. The extent of WEL formation is increased by Mn content and reduced by Ni and Co [27]. Work conducted by Ekberg [28] stated that R350HT rail develops a thicker WEL compared to R260 [29], suggesting that the original microstructure/chemistry of a rail affects

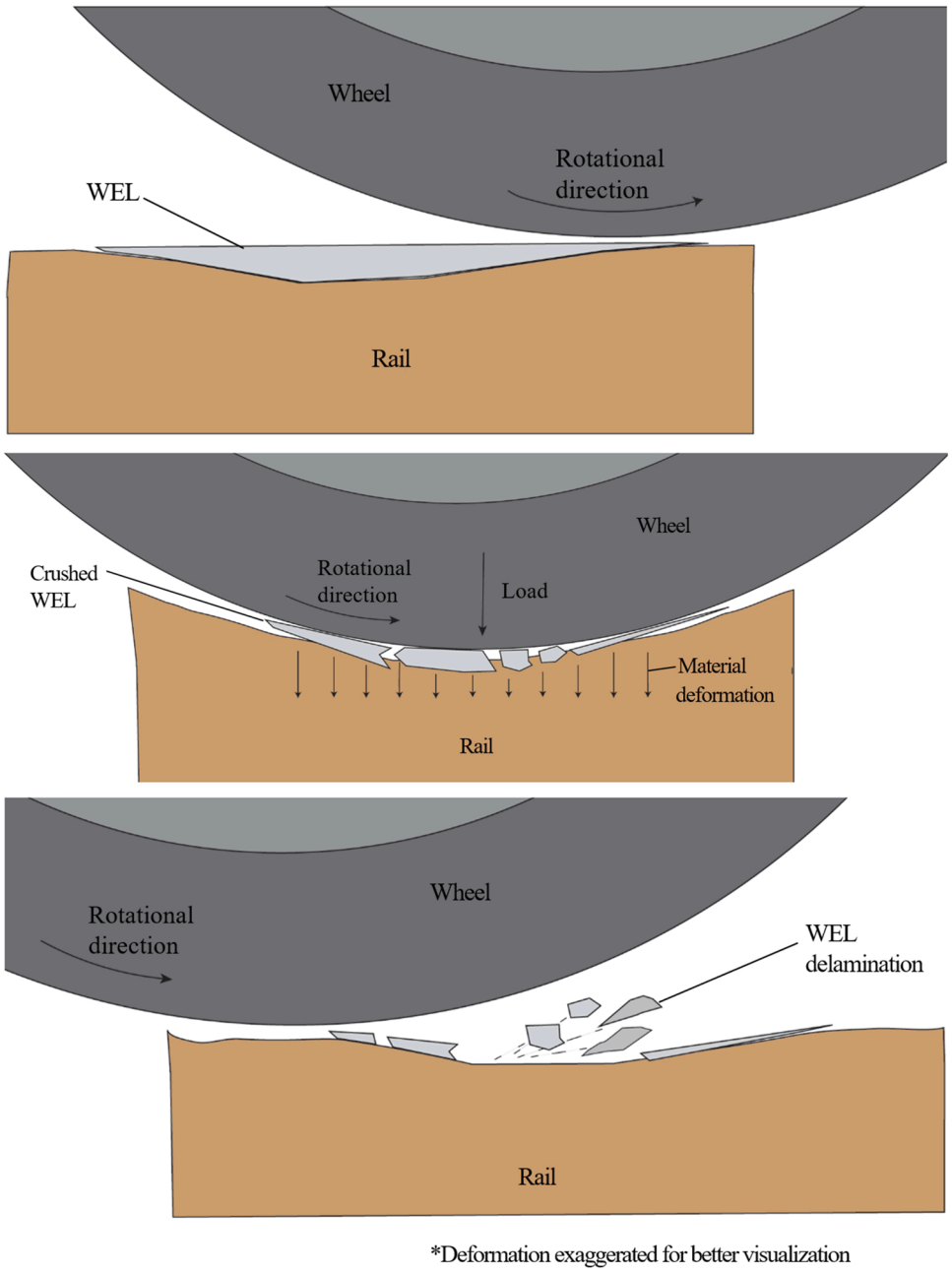

Fig. 16. Schematic illustration of WEL delamination during a wheel run-over.

the WEL formed. All these factors could lead to the formation of larger amounts of WEL on the R400HT sample.

The SEM images shown in Section 3.2 verified that cracks initiated within the WEL area can lead to the penetration of cracks through the deformed pearlite that is known as the transition zone. Research conducted by Carroll and Beynon [30] suggested that this crack propagation process below WELs was dependant on the ductility exhaustion of the subsurface pearlite on rails with non-continuous WEL [31]. The variation in ductility in the interfaces between WEL patches and pearlite results in dissimilar plastic deformation for each material, ultimately leading to the formation of cracks. This hypothesis can be applied for the results observed in the current study. Zhu et al. [32] found similar type of cracks in ex-service samples which induce squat type defects. It was reported that mild and moderate squats at the running band were found where a brittle WEL existed, and the cracks initiated from WEL were observed to have propagated through the transition zone into the rail matrix. As observed in other studies [32,17–19] using data from ex-service rails, similar outcomes were detected. Hence the cracks detected in this study could potentially grow further during the post grinding experiments penetrating the rail. This leads to the conclusion that WEL can affect harmfully the performance of a rail.

It was observed from the results 3.2.2 that the amount of WEL presented in the samples upon the completion of the experiments varied with the standard R260 specimen exhibiting the least amount. This comes in agreement with the results presented by Steenbergen et al. [33] where friction-induced martensite (FIM) was found to delaminate more easily on standard grades compared to heat-treated grades. As identical conditions were used in both grinding process and post-grinding testing the main distinguishable difference between the samples is their mechanical properties. Subsequently a reasonable explanation for this effect could be the ductility of the standard rails compared to the heat-treated rails. During the rolling/sliding process the wheel that is

over the martensite layer applies a force onto the surface. This results in compressive and tensile forces being generated in the top face and bottom surface of the rail structure. In standard grades, due to the ductility of the parent material, the bending is more significant in comparison to the heat treated rails leading to the breakage of the bonding between WEL and bulk material and eventually the delamination of the layer through the consecutive passes. An illustration of this theory is presented in Fig. 16. Similar to DLC (Diamond-like Carbon) coatings, the hardness gradient between WEL and bulk material interface can result in the delamination and premature fracture of the coating [34]. However, further investigation needs to take place to clearly conclude whether this hypothesis can be applied in different scenarios.

5. Conclusions

This study contributed to gaining considerable knowledge with regards to the performance of three rail grades after the grinding process. Experiments were done in full-scale testing facility with the aim of simulating the parameters existing in the field.

Analysis of the samples withdrawn from the field was done prior to the rolling/sliding experiments indicating the presence of WEL in all three grades R260, R350HT and R400HT. Furthermore, examples of WEL's brittle nature contributing to cracks propagation towards pearlite were discovered. It was also observed that WEL cavities were acting as intensified pressure points due the ductility dissimilarity between the pearlite and WEL resulting in the embedded WEL acting as a stress raiser and not allowing the stress to distribute uniformly compared to the surrounding surface.

The post-grinding experiments successfully imitate the conditions existing in the field. The results from the microstructural analysis of the samples showed that the WEL can contribute to the formation of cracks differently in each rail grade. The harder samples (R350HT and R400HT) due to their low ductility maintain the larger quantities of WEL after the completion of the experiments. This resulted in WEL being encapsulated by the deformed pearlite creating nucleation sites for cracks. On the other hand, very few instances of WEL near cracks were found in the R260 sample allowing the conclusion that the higher ductility and wear of softer materials can contribute to the delamination of WEL. This comes in agreement with the larger surface defects formed on the harder samples (R350HT and R400HT). It was found that the facet edges, the presence of WEL as well as the ductility of the material can affect this mechanism.

The wear rate against Tγ parameter was used to identify the performance against energy losses in each case. It was shown that the ground samples exhibited higher wear rates compared to non-ground samples from the same grade. Furthermore, roughness development was successfully monitored throughout the experiments. This allowed to detect the time required for each sample's roughness to reach stabilisation and the identification of run-in and wear regions.

Debris was collected throughout the experiments and analysed allowing the correlation of its size and morphology to the roughness data. It was proposed that this could be used as a tool for the identification of the run-in and wear regions throughout rail's usage. Nevertheless, further experiments need to take place to confidently use debris as an indication key for the rail running regions.

Declaration of Competing Interest

The authors declare that they have no known competing financial interests or personal relationships that could have appeared to influence the work reported in this paper.

Data availability

Data will be made available on request.

Acknowledgements

For the purpose of open access, the author has applied a 'Creative Commons Attribution (CC BY)* licence to any Author Accepted Manuscript version arising. The authors are grateful to the Royal Academy of Engineering for financial support through the Industry Academia Partnership Programme, project n. IAPP\1516\91, Metro de Medellín for providing rails and wheels for study, and Network Rail for partially funding this study.

References

[1] Al-Juboori A, et al. Characterisation of white etching layers formed on rails subjected to different traffic conditions. Wear 2019;vol. 436–437. https://doi.org/10.1016/J.WEAR.2019.202998.
[2] Stock R, Pippan R. RCF and wear in theory and practice-The influence of rail grade on wear and RCF. Wear 2011;vol. 271(1–2):125–33. https://doi.org/10.1016/J.WEAR.2010.10.015.
[3] Pointner P, Joerg A, Jaiswal J. "Deliverable Rep D4 1 5GL-Defin Guidel Use Differ rail grades INNOTRACK Guidel," 2009:45.
[4] Muhamedsalih Y, Hawksbee S, Tucker G, Stow J, Burstow M. Squats on the Great Britain rail network: Possible root causes and research recommendations. Int J Fatigue 2021;vol. 149:106267. https://doi.org/10.1016/J.IJFATIGUE.2021.106267.
[5] "Experimental analysis of the effect of the reprofiling process on wear and fatigue due to rail rolling contact in the wheel-rail system in the Medellín Metro." https://repositorio.unal.edu.co/handle/unal/49843 (accessed Aug. 17, 2022).
[6] Hardwick C, Lewis R, Eadie DT. Wheel and rail wear—Understanding the effects of water and grease. Wear 2014;vol. 314(1–2):198–204. https://doi.org/10.1016/J.WEAR.2013.11.020.
[7] Santa JF, et al. Twin disc assessment of wear regime transitions and rolling contact fatigue in R400HT – E8 pairs. Wear 2019;vol. 432–433:102916. https://doi.org/10.1016/j.wear.2019.05.031.
[8] Allan AM, Zarembski M. The art and science of rail grinding. Simmons-Board Books 2005.
[9] Cuervo PA, Santa JF, Toro A. Correlations between wear mechanisms and rail grinding operations in a commercial railroad. Tribol Int 2015;vol. 82(PB):265–73. https://doi.org/10.1016/j.triboint.2014.06.025.
[10] Zhou L, Brunskill HP, Lewis R. Real-time non-invasive measurement and monitoring of wheel–rail contact using ultrasonic reflectometry. Struct Heal Monit 2019;vol. 18(5–6):1953–65. https://doi.org/10.1177/1475921719829882.
[11] Lewis SR, et al. A Re-commissioned flexible full-scale wheel/rail test facility," Proc. 11th Int. Conf. Contact Mech. Wear Rail/Wheel Syst C 2018;2018:518–28.
[12] Buckley-Johnstone L, Harmon M, Lewis R, Hardwick C, Stock R. A comparison of friction modifier performance using two laboratory test scales. https://doi Org/10 1177/0954409718787045 . 2018;vol. 233(2):201–10. https://doi.org/10.1177/0954409718787045.
[13] Fukagai S, Brunskill HP, Hunter AK, Dwyer-Joyce RS, Lewis R. Transitions in rolling-sliding wheel/rail contact condition during running-in. Tribol Int 2019;vol. online 17. https://doi.org/10.1016/j.triboint.2019.03.037.
[14] Magel E, Roney M, Kalousek J, Sroba P. The blending of theory and practice in modern rail grinding. Fatigue Fract Eng Mater Struct 2003;vol. 26(10):921–9. https://doi.org/10.1046/j.1460-2695.2003.00669.x.
[15] Steenbergen M. Squat formation and rolling contact fatigue in curved rail track. Eng Fract Mech 2015;vol. 143:80–96. https://doi.org/10.1016/J.ENGFRACMECH.2015.05.060.
[16] Blau PJ. "A Model Run- Other Transit sliding Frict," 1986.
[17] Mesaritis M, et al. A laboratory demonstration of rail grinding and analysis of running roughness and wear. Wear 2020;vol. 456–457:203379. https://doi.org/10.1016/j.wear.2020.203379.
[18] "Rolling Contact Fatigue: A Comprehensive Review | FRA." https://railroads.dot.gov/elibrary/rolling-contact-fatigue-comprehensive-review (accessed Apr. 05, 2021).
[19] F. Fau and L. Fretwell-Smith, "Effect of grinding quality, lubrication quality and rail hardness on flaking defect initiation on high rails," 2015.
[20] Eadie DT, et al. The effects of top of rail friction modifier on wear and rolling contact fatigue: full-scale rail-wheel test rig evaluation, analysis and modelling. Wear 2008;vol. 265(9–10):1222–30. https://doi.org/10.1016/j.wear.2008.02.029.
[21] P.J. Blau, "Running-in," in Encyclopedia of Tribology, Q. J. Wang and Y.-W. Chung, Eds. Boston, MA: Springer US, 2013, pp. 2967–2969.
[22] Mikhin NM, Lyapin KS. Hardness dependence of the coefficient of friction. Sov Phys J 1970;vol. 13(3):317–21. https://doi.org/10.1007/BF00818317.
[23] TataSteel, "Review of anti Squat research," 2013.
[24] A. Athukorala, "Investigation of Wear and Ratcheting Response of Head-Hardened Australian Rail Steel under Conditions of Rolling Contact Fatigue," Queensland University of Technology, 2016.
[25] C.J. Rasmussen, "Grinding-induced Rolling Contact Fatigue in Rails [Powerpoint Presentation]," 2021.
[26] Zhu MH, Zhou ZR, Liu JJ. Current state of the research of tribological white layer. Tribol Mater Surf Interfaces 1999;vol. 19(3):281.

[27] Steenbergen M, Dollevoet R. On the mechanism of squat formation on train rails - Part I: origination. Int J Fatigue . 2013;vol. 47:361–72. https://doi.org/10.1016/j.ijfatigue.2012.04.023.
[28] Ekberg A. "D3 1- Enhanc Track Struct- Status, key Influ Parameters prioritised Areas Improv V 6," 2018:1–47.
[29] Gu KK, et al. Analysis on the effects of rotational speed of grinding stone on removal behavior of rail material. Wear 2015;vol. 342–343:52–9. https://doi.org/10.1016/j.wear.2015.08.008.
[30] Carroll RI, Beynon JH. Rolling contact fatigue of white etching layer: part 1: crack morphology. Wear 2007;vol. 262(9–10):1253–66. https://doi.org/10.1016/J.WEAR.2007.01.003.
[31] Clayton P, Allery MBP. Metallurgical aspects of surface damage problems in rails. Can Metall Q 1982;vol. 21(1):31–46. https://doi.org/10.1179/000844382795243803.
[32] Zhu H, et al. Understanding and treatment of squat defects in a railway network. Wear 2020;vol. 442–443(January):2019. https://doi.org/10.1016/j.wear.2019.203139.
[33] Steenbergen M. Rolling contact fatigue in relation to rail grinding. Wear 2016;vol. 356–357:110–21. https://doi.org/10.1016/j.wear.2016.03.015.
[34] Dalibón EL, Escalada L, Simison S, Forsich C, Heim D, Brühl SP. Mechanical and corrosion behavior of thick and soft DLC coatings. Surf Coat Technol 2017;vol. 312:101–9. https://doi.org/10.1016/J.SURFCOAT.2016.10.006.